

Wray 15-906: a candidate luminous blue variable discovered with *WISE*, *Herschel* and SALT

O. V. Maryeva,^{1,2*} V. V. Gvaramadze,^{2,3†} A. Y. Kniazev^{4,5,2} and L. N. Berdnikov²

¹*Astronomical Institute, Czech Academy of Sciences, Fričova 298, 251 65 Ondřejov, Czech Republic*

²*Sternberg Astronomical Institute, Lomonosov Moscow State University, Universitetskij Pr. 13, Moscow 119992, Russia*

³*E. Kharadze Georgian National Astrophysical Observatory, Abastumani 0301, Georgia*

⁴*South African Astronomical Observatory, PO Box 9, 7935 Observatory, Cape Town, South Africa*

⁵*Southern African Large Telescope Foundation, PO Box 9, 7935 Observatory, Cape Town, South Africa*

Accepted 2020 August 27. Received 2020 August 27; in original form 2020 May 12

ABSTRACT

We present the results of study of the Galactic candidate luminous blue variable Wray 15-906, revealed via detection of its infrared circumstellar shell (of ≈ 2 pc in diameter) with the *Wide-field Infrared Survey Explorer (WISE)* and the *Herschel Space Observatory*. Using the stellar atmosphere code *CMFGEN* and the *Gaia* parallax, we found that Wray 15-906 is a relatively low-luminosity, $\log(L/L_{\odot}) \approx 5.4$, star of temperature of 25 ± 2 kK, with a mass-loss rate of $\approx 3 \times 10^{-5} M_{\odot} \text{ yr}^{-1}$, a wind velocity of $280 \pm 50 \text{ km s}^{-1}$, and a surface helium abundance of 65 ± 2 per cent (by mass). In the framework of single star evolution, the obtained results suggest that Wray 15-906 is a post-red supergiant star with initial mass of $\approx 25 M_{\odot}$ and that before exploding as a supernova it could transform for a short time into a WN11h star. Our spectroscopic monitoring with the Southern African Large Telescope (SALT) does not reveal significant changes in the spectrum of Wray 15-906 during the last 8 yr, while the *V*-band light curve of this star over years 1999–2019 shows quasi-periodic variability with a period of ≈ 1700 d and an amplitude of ≈ 0.2 mag. We estimated the mass of the shell to be $2.9 \pm 0.5 M_{\odot}$ assuming the gas-to-dust mass ratio of 200. The presence of such a shell indicates that Wray 15-906 has suffered substantial mass loss in the recent past. We found that the open star cluster C1128-631 could be the birth place of Wray 15-906 provided that this star is a rejuvenated product of binary evolution (a blue straggler).

Key words: line: identification – circumstellar matter – stars: emission-line, Be – stars: evolution – stars: individual: Wray 15-906 – stars: massive

1 INTRODUCTION

Sky surveys produced by the *Spitzer Space Telescope* (Werner et al. 2004), the *Wide-field Infrared Survey Explorer (WISE)*; Wright et al. 2010) and the *Herschel Space Observatory* (Pilbratt et al. 2010) provide rich material for studying the interaction of massive and less massive stars with their environment. The high angular resolution and sensitivity of the data obtained by these space missions allowed ones to detect a huge number of previously unknown circumstellar nebulae (Gvaramadze, Kniazev & Fabrika 2010b; Mizuno et al. 2010; Wachter et al. 2010; Cox et al. 2012; Hutsemékers, Cox & Vamvatira-Nakou 2013), bow shocks (Gvaramadze et al. 2011; Peri et al. 2012; Cox et al. 2012; Kobulnicky et al.

2016), dust waves (Ochsendorf et al. 2014) and planetary nebulae (Kronberger et al. 2016). Follow-up spectroscopy of central stars associated with the newly detected nebulae and bow shocks led to the discovery of rare types of massive stars, such as the luminous blue variable (LBV) and Wolf-Rayet stars (e.g. Gvaramadze et al. 2009, 2010a; 2012; Wachter et al. 2010, 2011; Mauerhan et al. 2010; Stringfellow et al. 2012a,b; Burgemeister et al. 2013; Flagey et al. 2014; Silva et al. 2017; Cochetti et al. 2020), a massive spun-up and rejuvenated high-velocity runaway star (Gvaramadze et al. 2019a), a massive white-dwarf merger product (Gvaramadze et al. 2019b), and a post-very late thermal pulse star (Gvaramadze et al. 2019c).

Of the massive stars revealed through the detection of their circumstellar nebulae, perhaps the most interesting are the LBVs (Conti 1984; Humphreys & Davidson 1994).

* E-mail: olga.maryeva@asu.cas.cz (OVM)

† E-mail: vgvaram@mx.iki.rssi.ru (VVG)

The defining characteristics of this rare class of stars¹ are irregular changes in their spectral appearance and brightness on time-scales from months to tens of years, leading to blue-red-blue excursions on the Hertzsprung-Russell diagram and visual brightness variability by more than one mag (e.g. Humphreys & Davidson 1994; Stahl et al. 2001; van Genderen 2001; Weis & Bomans 2020). Another common characteristic of the majority of LBVs is the presence of pc-scale circumstellar nebulae of various shapes around them (Nota et al. 1995; Clark, Larionov & Arkharov 2005). Currently, about 70 per cent of Galactic bona fide LBVs are known to be associated with such nebulae (Kniazev et al. 2015).

However, despite the great interest in these stars it is not yet settled at what stage of the evolution of massive stars the LBV activity takes place and what role the duplicity of massive stars may play in the origin of this activity (e.g. Langer et al. 1994; Stothers & Chin 1996; Groh et al. 2014; Justham, Podsiadlowski & Vink 2014). Also, the driving mechanism(s) of the LBV activity, the role of this activity in the evolution of massive stars, and the initial masses of stars susceptible to this activity are still poorly understood and remain debated (e.g. Smith, Vink & de Koter 2004; Vink 2012; Smith 2014; Davidson 2020).

There are also known several dozens of stars with LBV-like spectra, which did not show major changes in their spectra and brightness and which are treated as candidate LBVs (cLBVs; Clark et al. 2005; Gvaramadze & Kniazev 2017; Richardson & Mehner 2018). Most of these stars are surrounded by compact nebulae similar to those detected around bona fide LBVs, which suggests that they might be either dormant or ex-LBVs (Bohannon 1997). Spectroscopic and photometric monitoring of cLBVs could potentially confirm that some of them are indeed bona fide LBVs, while discovery of new (c)LBVs may allow us to advance our understanding of the nature of the LBV phenomenon.

In this paper, we present the results of study of the new Galactic cLBV Wray 15-906, revealed through the detection of its circular circumstellar shell with *WISE* and *Herschel*. In Section 2, we present images of the shell and its central star at several wavelengths, and review the existing data on the star. In Section 3, we describe our spectroscopic observations of Wray 15-906 with the Southern African Large Telescope (SALT) and present its light curve based on archival and our own photometric observations. In Section 4, we derive fundamental parameters of Wray 15-906 using the stellar atmosphere code CMFGEN. In Section 5, we discuss the spectroscopic and photometric variability of this star. In Section 6, we discuss the evolutionary status and possible fate of Wray 15-906, estimate the mass of its circumstellar shell, and search for its possible birth cluster. We summarize in Section 7.

2 WRAY 15-906 AND ITS CIRCULAR CIRCUMSTELLAR SHELL

Wray 15-906 (also ALS 2533 and Hen 3-729) was identified as an emission-line star by Wray (1966). Later on, it was classified as a possible Wolf-Rayet star by Stephenson & Sanduleak (1971) and Stenholm (1975), and as a possible symbiotic star by Henize (1976). Although Wray 15-906 is indicated in the SIMBAD data base² as a possible Wolf-Rayet star, it remained unexplored until recently and its nature was unclear.

Wray 15-906 attracted our attention after we discovered a circular shell around it using *WISE* data (Kniazev & Gvaramadze 2015). Follow-up optical spectroscopy of Wray 15-906 with SALT in 2012 (Kniazev & Gvaramadze 2015) revealed a rich emission spectrum typical of hot LBV stars, which along with the presence of the circular circumstellar shell point to the possibility that this star is an LBV. Subsequent spectroscopic monitoring of Wray 15-906 (carried out in the period 2013–2016) and the available photometric data (covering the time period from 2001 to 2016), however, did not reveal significant changes in the spectrum and brightness of this star, which led us to consider it as a cLBV (Kniazev, Gvaramadze & Berdnikov 2017).

In Fig. 1, we show *Herschel* 160 and 70 μm , *WISE* 22 and 12 μm , Two-Micron All Sky Survey (2MASS; Skrutskie et al. 2006) K_s -band, and SuperCOSMOS H-alpha Survey (SHS; Parker et al. 2005) $\text{H}\alpha + [\text{N II}]$ images of the region containing Wray 15-906 and the nebula around it. In the discovery *WISE* 22 μm image³ (see Fig. 1), the nebula appears as a circular limb-brightened shell of angular radius of ≈ 1 arcmin, which at a distance of $d = 3.53$ kpc (see below) corresponds to ≈ 1 pc (which is typical of circumstellar shells around LBVs; e.g. Weis 2001). There is no obvious counterpart to the shell at shorter infrared wavelengths, but it is clearly visible in the 70 μm image obtained with the Photodetector Array Camera and Spectrometer (PACS) instrument on board the *Herschel Space Observatory* (Pilbratt et al. 2010). PACS 160 μm and *WISE* 12 μm images show that Wray 15-906 is surrounded by clumpy emission on all sides, but it is not clear whether it is physically associated with the star. Wray 15-906 was also covered by the Galactic Legacy Infrared Mid-Plane Survey Extraordinaire (GLIMPSE; Benjamin et al. 2003), carried out by the *Spitzer* Infrared Array Camera (IRAC; Fazio et al. 2004). The shell is not visible in none of the four (8, 5.8, 4.5 and 3.6 μm) images provided by this survey. It is also not visible in the SHS $\text{H}\alpha + [\text{N II}]$ image.

In Table 1 we summarize basic properties of Wray 15-906, which we will later use for spectral modelling and searching for possible birth cluster of the star. The coordinates, parallax and proper motion measurements are from the second *Gaia* Data Release (DR2; Gaia Collaboration et al. 2018), while the distance is derived from a simple inversion of the parallax. The B , V and I_c magnitudes were measured by us in the course of photometric monitoring of central stars of the infrared nebulae discovered with *Spitzer* and *WISE* (see Section 3.2). They were obtained closest in time (about one and half month earlier) to the spectrum of

¹ Only 17 bona fide LBVs are known to date in the Milky Way (Kniazev, Gvaramadze & Berdnikov 2015; Richardson & Mehner 2018).

² <http://simbad.u-strasbg.fr/simbad/>

³ Shown for the first time in Kniazev & Gvaramadze (2015).

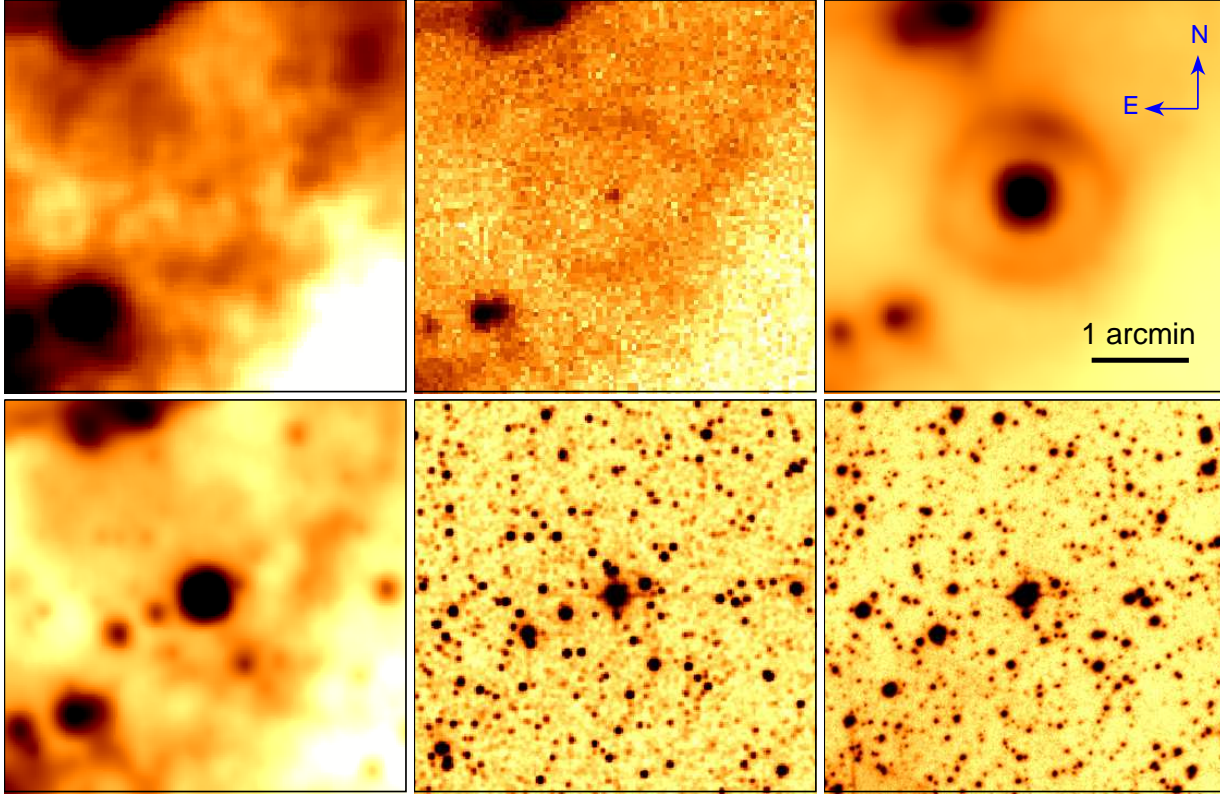


Figure 1. From left to right, and from top to bottom: *Herschel* PACS 160 and 70 μm , *WISE* 22 and 12 μm , 2MASS K_s -band and SHS $H\alpha$ + $[N\text{II}]$ images of the region containing Wray 15-906 and the shell around it (the scale and orientation of the images are the same). At a distance of 3.53 kpc, 1 arcmin corresponds to ≈ 1 pc.

Wray 15-906 used in Section 4.2 for spectral modelling. The J , H and K_s magnitudes are from the 2MASS All-Sky Catalog of Point Sources (Cutri et al. 2003). The *WISE* (3.4, 4.6, 12 and 22 μm) photometry is from the AllWISE Data Release (Cutri et al. 2014). The IRAC magnitudes at 3.6, 4.5, 5.8 and 8 μm are from the GLIMPSE Source Catalog (I+II+3D) (Spitzer Science Center 2009). Note the big difference between the *WISE* 3.4 μm and IRAC 3.6 μm magnitudes. Since it is unlikely that this difference is caused by the stellar variability (see Section 3.2) and because the *WISE* 3.4 μm magnitude better fits the spectral energy distribution (SED) of Wray 15-906 (see Section 4.2 and Fig. 6), we treat the IRAC 3.6 μm magnitude as unreliable.

Note also that the distance error bar given in Table 1 corresponds to the formal 1σ uncertainty of the parallax. In fact, the range of allowed distances to Wray 15-906 should be much broader because of the large astrometric excess noise of this star (e.g. Lindegren et al. 2018; Smith et al. 2019), which is only about 1.6 times less than the parallax and about 3.6 times larger than the parallax uncertainty (Gaia Collaboration et al. 2018). Thus, the distance given in Table 1 should be considered as a crude estimate, which hopefully will be better constrained by the forthcoming third *Gaia* data release.

Table 1. Properties of Wray 15-906.

RA(J2000)	$11^{\text{h}}54^{\text{m}}43^{\text{s}}.54$	<i>Gaia</i> DR2
Dec.(J2000)	$-63^{\circ}13'31''.1$	<i>Gaia</i> DR2
l	296 $^{\circ}$ 5959	<i>Gaia</i> DR2
b	$-1^{\circ}0534$	<i>Gaia</i> DR2
π (mas)	0.2835 ± 0.0495	<i>Gaia</i> DR2
μ_{α} (mas)	-5.820 ± 0.090	<i>Gaia</i> DR2
μ_{δ} (mas)	1.158 ± 0.071	<i>Gaia</i> DR2
d (kpc)	$3.53^{+0.74}_{-0.53}$	<i>Gaia</i> DR2
B (mag)	14.34 ± 0.03	This paper
V (mag)	12.50 ± 0.03	This paper
I_c (mag)	9.86 ± 0.02	This paper
J (mag)	7.70 ± 0.02	2MASS
H (mag)	6.87 ± 0.03	2MASS
K_s (mag)	6.24 ± 0.03	2MASS
3.4 μm (mag)	5.35 ± 0.18	<i>WISE</i>
3.6 μm (mag)	7.26 ± 0.32	<i>Spitzer</i> IRAC
4.5 μm (mag)	4.99 ± 0.05	<i>Spitzer</i> IRAC
4.6 μm (mag)	4.69 ± 0.09	<i>WISE</i>
5.8 μm (mag)	4.60 ± 0.03	<i>Spitzer</i> IRAC
8 μm (mag)	4.18 ± 0.03	<i>Spitzer</i> IRAC
12 μm (mag)	3.99 ± 0.02	<i>WISE</i>
22 μm (mag)	2.97 ± 0.03	<i>WISE</i>

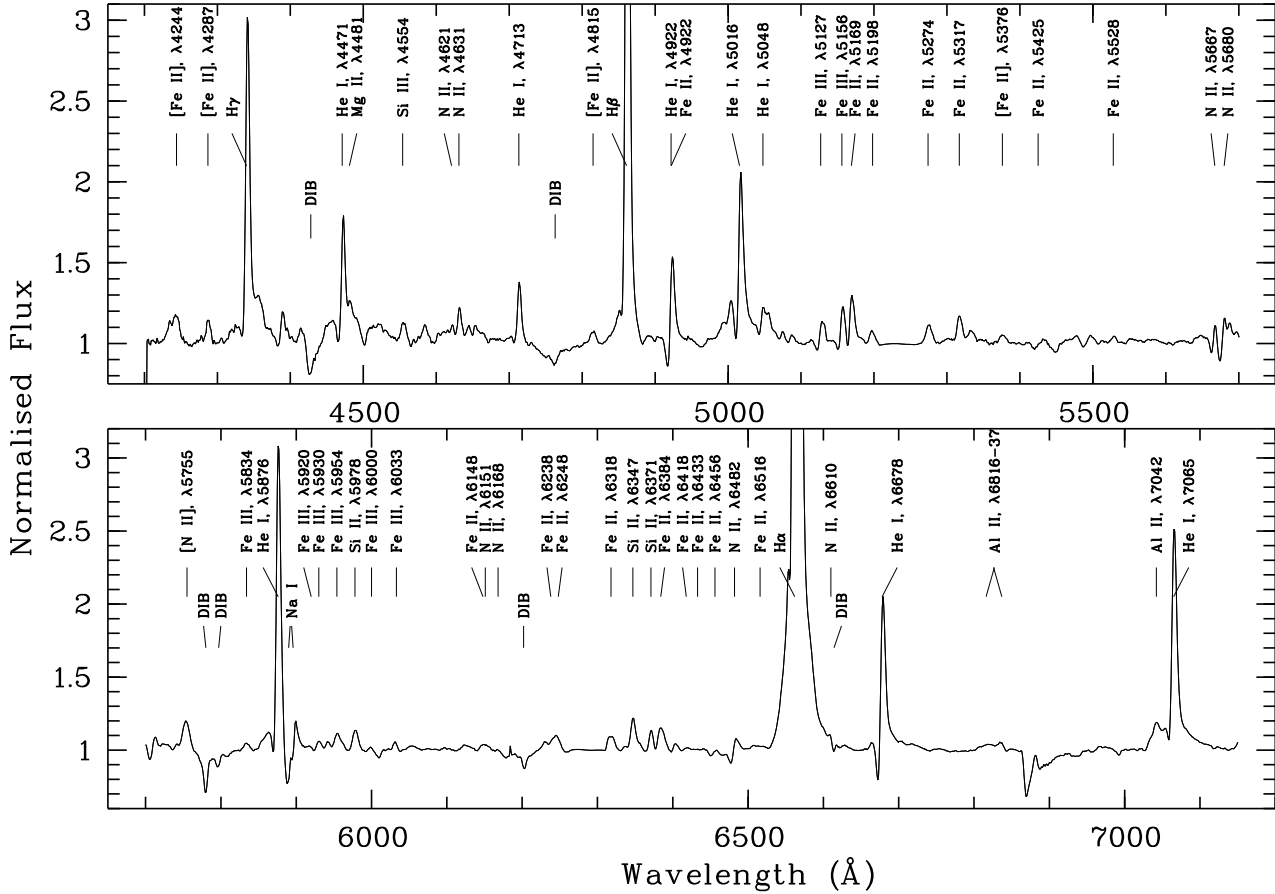


Figure 2. RSS spectrum of Wray 15-906 obtained on 2012 February 19, with the major lines and diffuse interstellar bands (DIBs) identified.

Table 2. Journal of the SALT RSS and HRS observations of Wray 15-906.

Spectrograph	Date	Exposure (sec)	Spectral scale (\AA pixel^{-1})	Resolving power	PA ($^\circ$)	Seeing (arcsec)	Spectral range (\AA)
RSS	2012 February 19	60+300	0.97	1000	0	1.2	4200–7300
RSS	2013 April 22	10+300	0.97	1000	42	1.6	4200–7300
RSS	2013 May 25	60+300	0.97	1000	42	2.4	4200–7300
RSS	2013 June 22	60+600	0.97	1000	42	1.7	4200–7300
RSS	2014 March 14	10+300	0.97	1000	316	2.0	4200–7300
RSS	2015 May 27	10+300	0.97	1000	136	2.4	4200–7300
HRS	2015 June 13	1200	0.04	16 000	–	3.0	3700–8900
HRS	2016 May 5	1200	0.04	16 000	–	3.0	3700–8900
HRS	2017 April 16	1200	0.04	16 000	–	3.0	3700–8900
HRS	2019 February 18	1200	0.04	16 000	–	3.0	3700–8900
HRS	2020 February 4	2400	0.04	16 000	–	3.0	3700–8900

3 OBSERVATIONS

3.1 Spectroscopy

We obtained our first spectrum of Wray 15-906 (Fig. 2) on 2012 February 19 on SALT (Buckley, Swart & Meiring 2006; O’Donoghue et al. 2006). The observation was carried out with the Robert Stobie Spectrograph (RSS; Burgh et al.

2003; Kobulnicky et al. 2003) in the long-slit mode. As expected, the spectrum turned out to be interesting (namely, similar to that of the bona-fide LBV P Cygni), so that we continued our observations in the following years in the hope of finding significant changes in it. In 2013–2015 we obtained five more RSS spectra of Wray 15-906.

All RSS spectra were taken with a slit width of 1.25 arc-

sec and with the PG900 grating, which covers the spectral range of 4200–7300 Å. This choice of the slit width and grating provides a final reciprocal dispersion of $0.97 \text{ \AA pixel}^{-1}$ and spectral resolution FWHM of 4.4–4.7 Å ($R \approx 1000$). The observations were done with a short (10 or 60 s) and long (300 or 600 s) exposures to exclude possible saturation of strong emission lines. An Xe lamp arc spectrum (taken immediately after the science frames) was used for wavelength calibration. The relative flux calibration was performed using observations of spectrophotometric standard stars. A comparison of the obtained spectra revealed only slight changes in their appearance.

In 2015 the High Resolution Spectrograph (HRS; Barnes et al. 2008; Bramall et al. 2010, 2012; Crause et al. 2014) was commissioned at the SALT, which allowed us to continue monitoring of Wray 15-906 with a much better spectral resolution. We used this fibre-fed, high dispersion échelle spectrograph in the low resolution mode ($R \approx 16\,000$) to obtain spectra in the blue and red arms over the total spectral range of $\approx 3700\text{--}8900 \text{ \AA}$. The CCDs of both arms were read out by a single amplifier with a 1×1 binning. Four spectra of Wray 15-906 were taken in 2015–2019 with the same exposure time of 1200 s, and one more spectrum on 2020 February 4 with the exposure time of 2400 s. Three arc spectra of ThAr lamp and three spectral flats were obtained for each observation under the same resolution mode during a weekly set of HRS calibrations. The spectrum obtained in 2016 was used in Section 4.2 for spectral modelling and its portions are shown in Figs 4 and 5.

The log of our spectroscopic observations is given in Table 2.

The primary reduction of the RSS and HRS spectra was performed using the SALT science pipeline (Crawford et al. 2010). For further reduction of the long-slit data we followed the procedure described in Kniazev et al. (2008). The HRS spectra were further reduced using the MIDAS HRS pipeline described in detail in Kniazev, Gvaramadze & Berdnikov (2016) and Kniazev et al. (2019).

3.2 Photometry

As a part of our photometric observations of central stars of the infrared nebulae detected with *Spitzer* and *WISE*, we determined B , V and I_c magnitudes of Wray 15-906 on CCD frames obtained with the South African Astronomical Observatory (SAAO) 76-cm and 1-m telescopes in 2011–2016. We used an SBIG ST-10XME camera equipped with filters of the Kron-Cousins system (see Berdnikov et al. 2012).

To construct the long-term light curve of Wray 15-906, we also collected V -band photometry of this star from the All Sky Automated Survey (ASAS; Pojmanski 1997) and the All-Sky Automated Survey for Supernovae (ASAS-SN; Shappee et al. 2014; Kochanek et al. 2017), as well as that obtained by the Optical Monitoring Camera (OMC; Alfonso-Garzón et al. 2012) on board the International Gamma-Ray Astrophysics Laboratory *INTEGRAL* observatory.

From the ASAS survey we used only ‘grade A’ data with accuracy of $\approx 0.04\text{--}0.07$ mag. From the ASAS-SN and OMC photometry we selected the data points with accuracy better than 0.02 and 0.1 mag, respectively. Altogether, we collected 857 measurements covering the years 1999–2019.

The resulting V -band light curve for Wray 15-906 is presented in Fig. 3. One can see that Wray 15-906 experiences a quasi-periodic brightness variability of several tenths of mag around the average value of $V = 12.35 \pm 0.11$ mag (see also Section 5.2).

4 SPECTRAL ANALYSIS AND STELLAR PARAMETERS

4.1 The stellar spectrum

Wray 15-906 displays a rich emission-line spectrum, dominated by strong Balmer and He I lines, all of which have P Cygni profiles (see Figs 4 and 5). No He II lines are detected neither in the RSS, nor in the HRS spectra. Other detected emission lines are due to N II (all show P Cygni profiles), Fe II and III, Si II and III, Al II and Mg II. Like in P Cygni and several other (c)LBVs (Stahl et al. 1993; Gvaramadze et al. 2010a; 2012a), the Fe III lines with low multiplet numbers show clear P Cygni profiles, while those with higher multiplet numbers are fully in emission. The near-infrared part of the HRS spectra shows Paschen lines in emission and emission lines of neutral nitrogen (N I $\lambda 8682$) and oxygen (O I 7772-5, 8446). The spectra also show the prominent forbidden line of [N II] $\lambda 5755$ and numerous forbidden lines of singly-ionized iron. In the HRS spectra these lines have a flat-topped appearance (see Figs 5 and 8).

In Fig. 4, we show the blue region of the HRS spectrum of Wray 15-906 obtained on 2016 May 5 and compare it with spectra of the bona-fide LBV P Cygni and the WN11h (Smith, Crowther & Prinja 1994; Walborn & Fitzpatrick 2000) star Wray 15-682 (Hen 3-519, WR31a)⁴. One can see that the three spectra bear a strong resemblance with each other. The main difference is that Wray 15-906, like P Cygni, has no He II lines, meaning that it is a P Cygni-type B supergiant. On the other hand, the emission lines in Wray 15-906 and Wray 15-682 are much broader than in P Cygni, indicating that the wind velocity in the former two stars is higher than that in the latter one. The results of our spectral modelling (see the next section) show that Wray 15-906 is a blueward evolving post-red supergiant star and that its temperature (25 ± 2 kK) is a bit lower than that of Wray 15-682 (27 ± 1 kK; Smith et al. 1994). This implies that Wray 15-906 is on the more advanced evolutionary stage than P Cygni and that soon it could turn into a WN11h star and explode as a supernova (see Section 6.1).

4.2 Spectral modelling

The basic parameters of Wray 15-906 were determined by means of the CMFGEN code of Hillier & Miller (1998), which was developed to solve radiative transfer equations for objects with spherically symmetric extended outflows using the full comoving-frame formulation of the radiative transfer equation (e.g. Hillier et al. 2001; Najarro et al. 2009; Groh et al. 2009b). CMFGEN incorporates line blanketing, the effects of clumping and Auger ionization. Every model is

⁴ The spectrum of P Cygni is taken from the ELODIE archive (Moultaka et al. 2004) at Observatoire de Haute-Provence, while that of Wray 15-682 is from Smith et al. (1994).

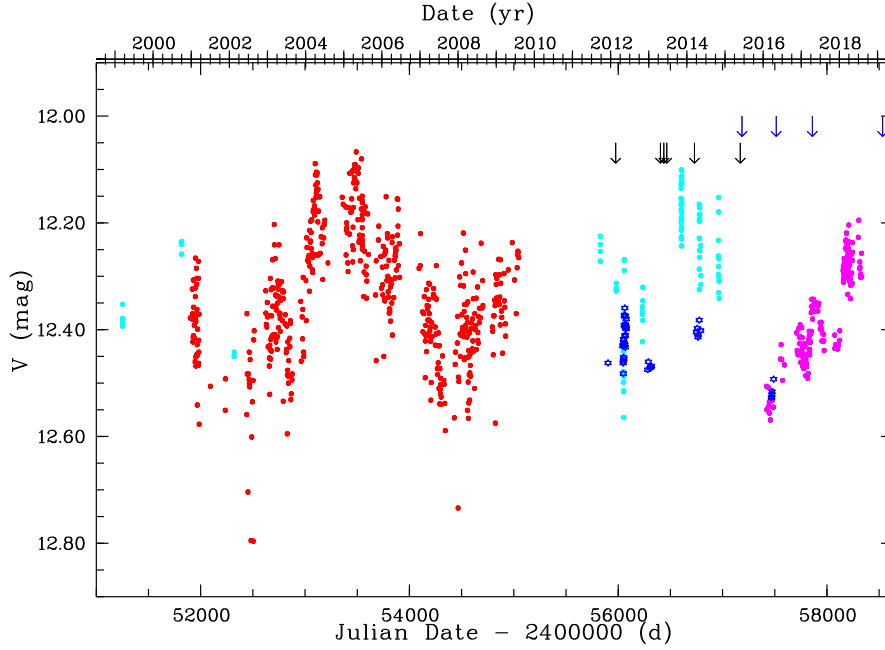


Figure 3. *V*-band light curve of Wray 15-906 as a function of time over years 1999–2019. Red, cyan and magenta dots correspond, respectively, to the ASAS, OMC and ASAS-SN photometry. Our measurements are shown with open blue hexagons. The arrows mark the dates of the RSS (bottom row) and HRS (upper row) spectra obtained in 2012–2019.

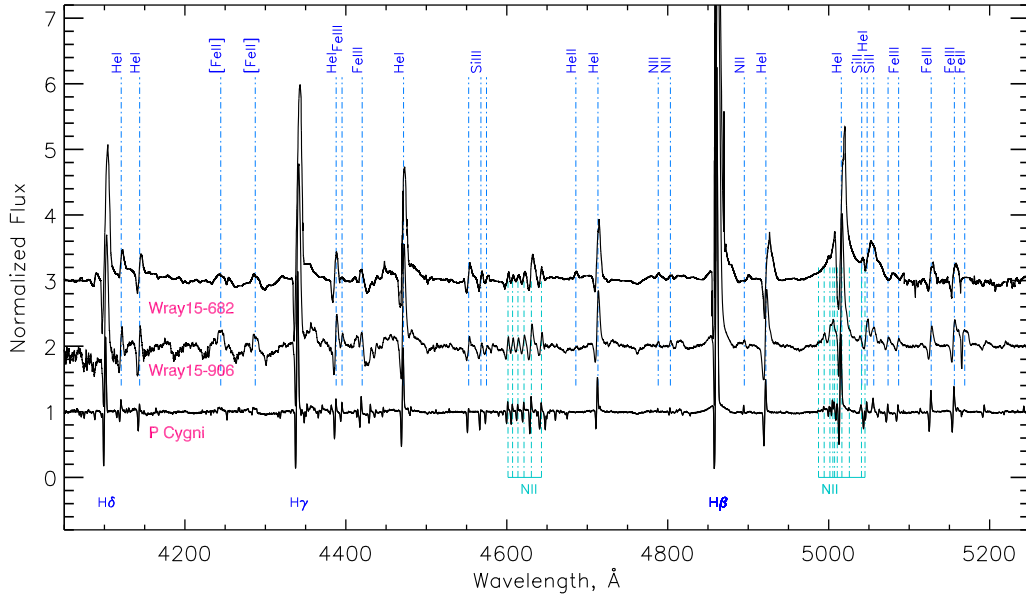


Figure 4. Comparison of a normalized portion of the HRS spectrum of Wray 15-906 taken on 2016 May 5 with corresponding parts of spectra of the Galactic bona fide LBV P Cygni and the WN11h star Wray 15-682.

characterized by a set of parameters, such as the hydrostatic stellar radius R_* , luminosity L_* , mass-loss rate \dot{M} , volume filling factor f , wind terminal velocity v_∞ , stellar mass M_* , and abundances Z_i of elementary species (our modelling included H, He, C, N, O, Ne, Mg, Al, Si, S, Ar, Ca and Fe). Fig. 5 shows the comparison of the best-fitting model spec-

trum with the normalized HRS spectrum obtained on 2016 May 5. As the length of the HRS échelle orders is $\approx 140 \text{ \AA}$, the continuum normalization was straightforward even in the region of the $H\alpha$ line with its wide ($\approx 60 \text{ \AA}$) wings. The spectrum was independently normalized manually by two

co-authors using the MIDAS and DECH30⁵ software packages. Dividing one normalized spectrum by another showed that they are consistent with each other to within 5 per cent. This makes us confident that the normalization procedure does not significantly affect the line wings and the results of our modelling.

The modelling proceeded in several steps (cf. Gvaramadze et al. 2018). First, we derived the temperature T_* at the hydrostatic radius and the temperature T_{eff} at the radius $R_{2/3}$ where the Rosseland optical depth is equal to 2/3. For this, we used the intensities of the Si II–III, Fe II–III, He I and N I–II lines.

Then, we derived the colour excess $E(B - V)$ of the star of 2.07 mag. For this, we adjusted the observed SED with the model spectrum scaled to the *Gaia* DR2 distance to Wray 15-906 of $d = 3.53$ kpc (see Fig. 6). We used the extinction law from Fitzpatrick (1999) with a total-to-selective absorption ratio of $R_V = 3.1$. Note that although R_V was found to vary from 2.2 to 5.8 between different lines of sight in the Milky Way (Fitzpatrick, 1999), the observed SED was fitted pretty well without need to assume a peculiar reddening law.

Next, we determined the radius (and luminosity) of Wray 15-906. For this, we compared the observed SED with the synthetic spectrum calculated for the adopted distance, corrected for interstellar reddening and convolved with the transmission curves of the standard Johnson B , V and I_c filters.

On the next step, v_∞ and \dot{M} were estimated by using the lines with P Cygni-type profiles and intensities of the emission lines. CMFGEN allows us to build models with different velocity laws describing the radial dependence of the wind velocity. For Wray 15-906 we found it sufficient to use a wind velocity law exponent of $\beta = 1$.

As a final step, we derived abundances of hydrogen, helium, nitrogen and oxygen. The H and He abundances were derived by iterative adjustment of the He-to-H abundance ratio and other fundamental parameters of Wray 15-906 to reproduce the overall shape of all detected lines of these elements. The N abundance was derived by analysing the behaviour of the N II and N I lines, while the O I lines in near-infrared part of the spectrum were used to estimate the O abundance. Since no carbon lines were detected in the spectrum, for this element we derived only an upper limit on its abundance by decreasing its value until the C II $\lambda\lambda 7231$ –36–37 lines disappear in the model spectrum. From the large number of Si and Mg lines we estimated the abundances of these elements to be around the solar ones. For other elements in our models we adopted their solar abundances; in the CMFGEN code the solar abundances are taken from Cox (2000).

The stellar wind was assumed to be clumpy with a void interclump medium (Hillier & Miller 1999). The wind volume filling factor $f(r) = \bar{\rho}/\rho(r)$, where $\bar{\rho}$ is the homogeneous (unclumped) wind density and $\rho(r)$ is the density in clumps (assumed to be optically thin), depends on radius as $f(r) = f_\infty + (1 - f_\infty)\exp(-v(r)/v_{\text{cl}})$, where f_∞ characterize the density contrast and v_{cl} is the velocity at which clumping starts. In our modelling, we adopted $f_\infty = 0.1$ and

Table 3. Stellar parameters of Wray 15-906 for three distances (see the text for details).

d (kpc)	3.00	3.53	4.27
$\log(L_*/L_\odot)$	5.19 ± 0.02	5.38 ± 0.02	5.50 ± 0.02
\dot{M} ($10^{-5} M_\odot \text{ yr}^{-1}$)	2.8 ± 0.3	3.3 ± 0.3	4.0 ± 0.3
R_* (R_\odot)	21.0 ± 4.4	26.1 ± 5.0	30.1 ± 5.6
T_{eff} (kK)	18.7 ± 1.5	19.2 ± 1.5	20.1 ± 1.5
$R_{2/3}$ (R_\odot)	37.5	44.3	46.3
T_* (kK)		25 ± 2	
v_∞ (km s^{-1})		280 ± 50	
β (adopted)		1.0	
f (adopted)		0.1	
H/He		2.15 ± 0.15	
H (mass fraction)		0.35 ± 0.02	
He (mass fraction)		0.65 ± 0.02	
C (mass fraction)		$\leq 6 \times 10^{-5}$	
N (mass fraction)		$(2.7 - 3.5) \times 10^{-3}$	
O (mass fraction)		$(0.8 - 1.6) \times 10^{-4}$	
$E(B - V)$ (mag)		2.07	
R_V (adopted)		3.1	

$v_{\text{cl}} = 50 \text{ km s}^{-1}$. We also calculated models with higher values of f_∞ of 0.25 and 0.5. However, the increase of the wind homogeneity leads to the increase of the influence of electron scattering on line profiles (Hillier 1991) and to the disappearance of absorption components in the H α and H β lines (cf. Groh et al 2009b), which is not consistent with the observed spectrum. Correspondingly, we used $f_\infty = 0.1$ in the final model. Puls et al. (2006) studied the radial stratification of clumping in hot star winds by simultaneous modelling of H α , infrared, mm and radio data, and demonstrated that for dense winds it decreases outwards (see also Najarro, Hanson & Puls 2011). And indeed our computations show that for simultaneous fitting of the visible and near-infrared parts of the spectrum the clumping has to start to disappear at the distance where the wind velocity exceeds 200 km s^{-1} .

The derived parameters are listed in Table 3 for three distances to Wray 15-906, derived from the *Gaia* DR2 parallax and its ± 1 -sigma values (see Table 1).

We also measured the heliocentric radial velocity, $v_{r,\text{hel}}$, of the [N II] $\lambda 5755$ line using all five HRS spectra. It is believed that this velocity corresponds to the systemic velocity of the star (Stahl et al. 2001). The measurements (made using the programs described in Kniazev et al. 2004) are listed in Table 4. It appears that $v_{r,\text{hel}}$ changes slightly around zero. We fit these measurements to a sine curve using the χ^2 algorithm. The best-fitting result⁶ ($\chi^2 = 7 \times 10^{-4}$) is shown in Fig. 7. It indicates that $v_{r,\text{hel}}$ changes with a period of 140.21 ± 0.01 d and an amplitude of $7.17 \pm 0.01 \text{ km s}^{-1}$, and implies a systemic radial velocity of $-0.07 \pm 0.01 \text{ km s}^{-1}$. We speculate that these changes could be due to pulsations in the stellar atmosphere (cf. Section 6.1).

⁵ <http://gazinur.com/DECH-software.html>

⁶ We caution that this result is not unique due to the limited number of data points.

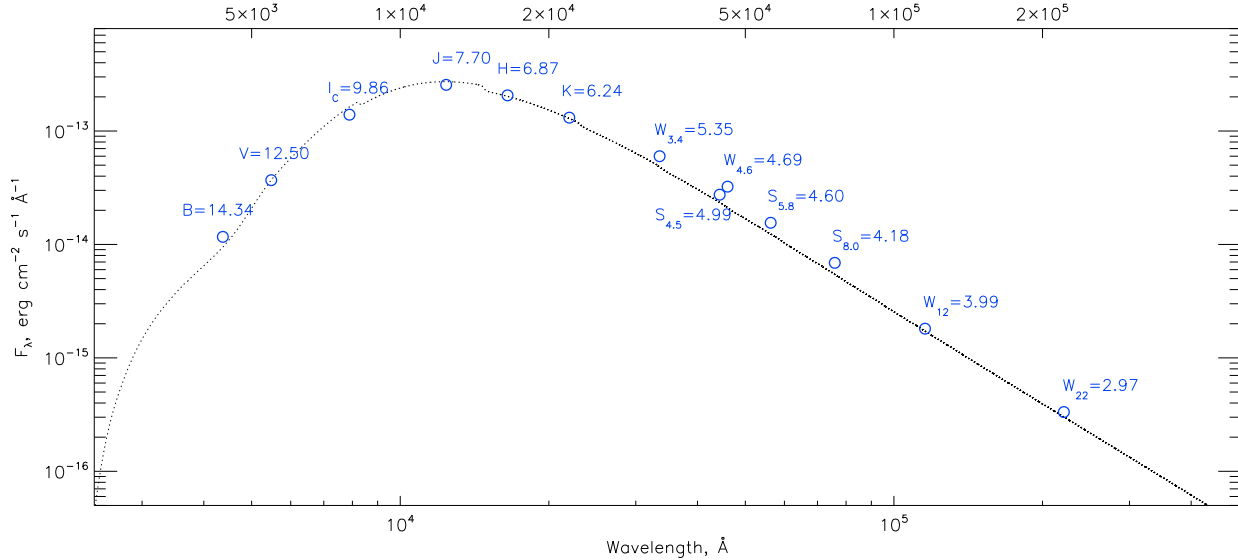


Figure 6. Observed flux distribution of Wray 15-906 (open circles) based on the photometric data from Table 1, compared to the continuum of the reddened model spectrum (dotted line) with the parameters as given in Table 3.

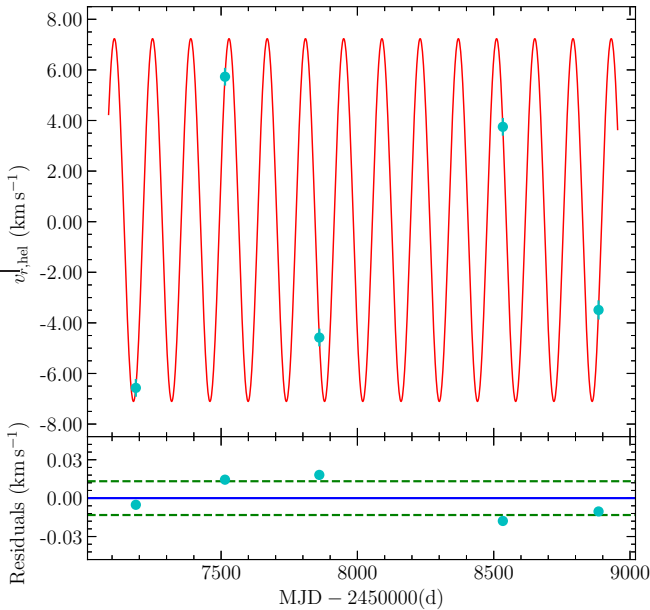


Figure 7. Changes in the heliocentric radial velocity of the [N II] $\lambda 5755$ line in the spectrum of Wray 15-906. Note that the uncertainties in the data points are very small.

Table 4. Changes in the heliocentric radial velocity of the [N II] $\lambda 5755$ line in the spectrum of Wray 15-906.

Date	JD	$V_{r, \text{hel}}$ (km s $^{-1}$)
2015 June 13	2457187.25163	-6.57 ± 0.35
2016 May 5	2457514.29555	5.73 ± 0.35
2017 April 16	2457860.25479	-4.58 ± 0.35
2019 February 18	2458533.48539	3.75 ± 0.35
2020 February 4	2458884.49809	-3.49 ± 0.38

5 SPECTROSCOPIC AND PHOTOMETRIC VARIABILITY OF WRAY 15-906

5.1 Spectroscopic variability

As noted in Section 2, our initial spectroscopic monitoring did not detect significant changes in the spectrum of Wray 15-906 in 2012–2016. Moreover, the spectrum did not change much in the following 4 yr. Particularly, the He II and N III lines did not appear in none of the RSS and HRS spectra, meaning that the stellar effective temperature remains nearly constant during the 8 yr of observations. Similarly, inspection of the HRS spectra did not reveal noticeable changes in the width of flat-topped forbidden lines (see the bottom row in Fig. 8). Since the width of these lines is a good measure of the terminal wind velocity (cf. Stahl et al. 1991, 2001), we conclude that v_∞ did not change as well. From the radial velocities of the blue and red edges of the flat-topped lines, we estimated the wind expansion velocity to be 275 ± 30 km s $^{-1}$, which agrees well with the wind velocity of 280 ± 50 km s $^{-1}$ derived in Section 4.2.

On the other hand, the comparison of the spectra revealed moderate variability in the line intensities and P Cygni profiles, which is more obvious in the HRS spectra. This variability is demonstrated in Fig. 8 where we plot profiles of selected lines from five HRS spectra obtained during the last 4.5 yr. Fig. 8 shows that lines experience two types of variability, both of which are typical of hot stars with extended atmospheres (Lamers, Korevaar & Cassatella 1985; Kaufer et al. 1996; Markova & Valchev 2000; Stahl et al. 2001; Chentsov & Maryeva 2016).

First of them is the variability of line intensities, more prominent in the Balmer lines (upper row in Fig. 8). Particularly, one can see that the intensity of the H α line was weakly variable in 2015–2018 and increased by ≈ 50 per cent during the last year. This type of variability could be attributed to changes in the mass-loss rate, possibly caused

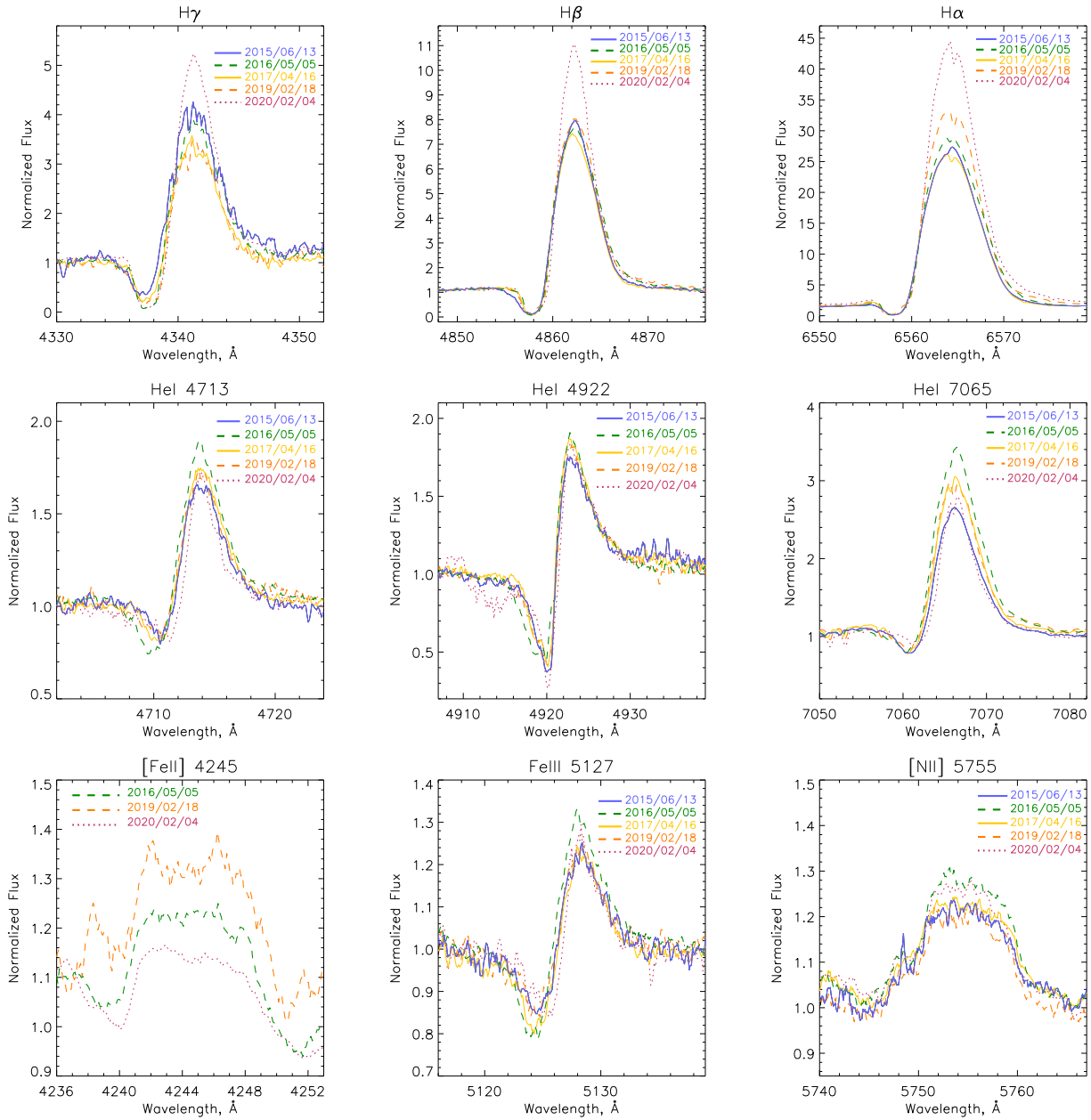


Figure 8. Line profiles variability in the HRS spectra of Wray 15-906. The dates of observations are indicated in the legends.

by the bi-stability jump (Pauldrach & Puls 1990) or/and stellar pulsations (see Section 6.1).

The second type of variability is characterized by the appearance of additional components in the P Cygni absorption profile of some lines, e.g. He I λ 5016 and Fe II λ 5169 (see Fig. 9). It could be connected with variability of the line-of-sight optical depth of the stellar wind caused by the presence of a large scale spiral-shaped pattern within the wind. Such a pattern could arise from interaction of flows of different speed in non-spherically symmetric stellar winds (e.g. Kaper et al. 1996; Fullerton et al. 1997). Appearance of additional P Cygni absorption components could also be connected to abrupt changes in the wind structure caused by the bi-stability jump (Groh & Vink 2011), while in binary

systems they could originate in the wind-wind interaction zone (Lobel et al. 2015).

5.2 Photometric variability

To search for a possible periodicity in the light curve of Wray 15-906, we computed its Lomb-Scargle (LS) periodogram (Lomb 1976; Scargle 1982) using the MIDAS context TSA. The resulting LS periodogram shows numerous spikes, of which the strongest ones are located in the region with periods > 100 d. This part of the periodogram is shown in Fig. 10. The most prominent spike corresponds to the period of $P_1 = 1698 \pm 9$ d. In the upper panel of Fig. 11, we superimposed a sine wave with this period (red dashed line)

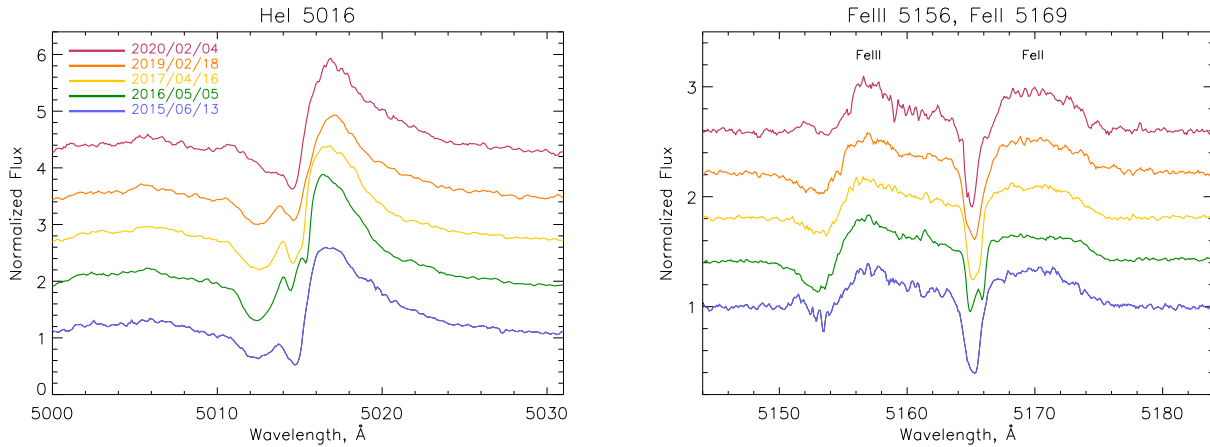


Figure 9. Changes in the absorption components of the He I λ 5016 and Fe II λ 5169 lines in the HRS spectra taken in 2015–2020.

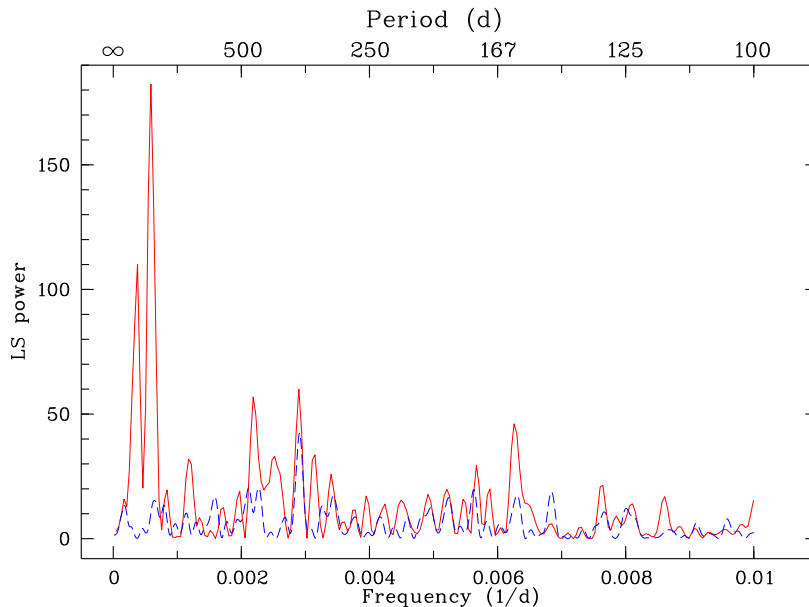


Figure 10. A part of the Lomb-Scargle (LS) periodogram of the light curve of Wray 15-906 from 1999–2019 showing the strongest power spikes (red solid line). The dashed blue line corresponds to the LS periodogram after subtraction of the three strongest spikes at periods of 1698, 2818 and 395 d.

on the observed light curve (black dots) to show that they agree quite well with each other.

After subtraction of this period from the LS periodogram, we found the next strongest spike at $P_2 = 2818 \pm 110$ d. Repeating the subtraction procedure leads to the detection of the third period of $P_3 = 395.31 \pm 0.22$ d. The LS periodogram after subtraction of the three periods is shown in the inset to Fig. 10 with the dashed (blue) line.

Using the detected three periods, we fit the observed light curve with a linear combination of three sine waves with amplitudes $A_1 = 0.112 \pm 0.004$ mag, $A_2 = 0.038 \pm 0.004$ mag and $A_3 = 0.025 \pm 0.003$ mag. The resulting synthetic light curve is shown with a solid blue line in the upper panel of Fig. 11. The bottom panel of Fig. 11 shows residuals of the fit (the dispersion of the residuals is 0.07 mag).

Then, we re-analysed the light curve after excluding

data points with the lowest accuracy (i.e. the OMC photometry). In this case, the LS periodogram shows the strongest power spike at a period of 1729 ± 3 d, which is almost identical to the period P_1 , while the two other strongest spikes were found at periods of 7422 ± 20 and 289 ± 4 d. This exercise confirms that the period of ≈ 1700 d is indeed present in the light curve, and suggests that the other two periods are rather spurious. Although it is not clear what the origin of the ≈ 1700 d period, it is tempting to assume that it is due to possible duplicity of the star, i.e. related to the orbital period of the binary system. Further coordinated photometric and spectroscopic observations of Wray 15-906 along with long baseline interferometric imaging are needed to confirm or reject this assumption (cf. Richardson, Gies & Williams 2011; Boffin et al., 2016).

Also, we used our photometric observations in 2011–

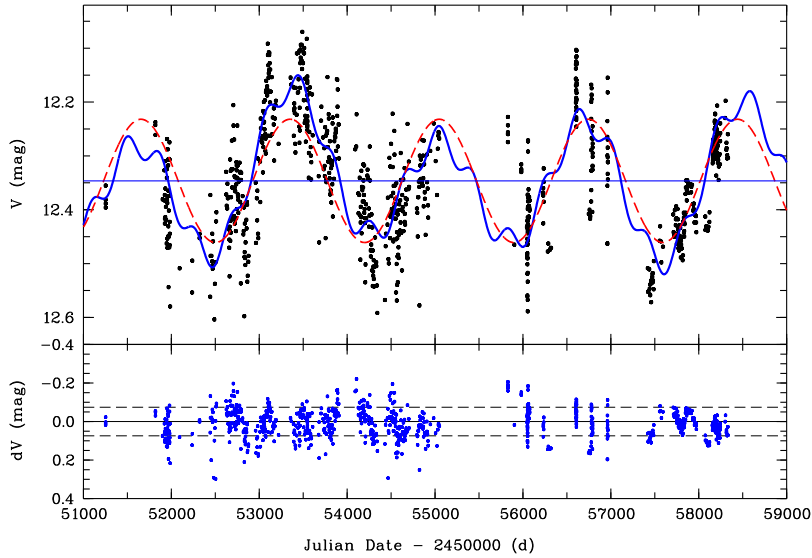


Figure 11. Upper panel: the fit to the observed light curve of Wray 15-906 with three sine waves of period 2818, 1698 and 395 d. The observed light curve is shown with the black dots. The fit to the data is shown with the solid (blue) curve. The dashed (red) sine wave corresponds to the strongest power spike in the LS periodogram at the period of 1698 d. The horizontal (blue) line shows the average V magnitude of 12.35 ± 0.11 . Bottom panel: residuals of the fit. The mean residual magnitude and its 1σ uncertainty of 0.07 mag are shown with the solid and dashed lines, respectively.

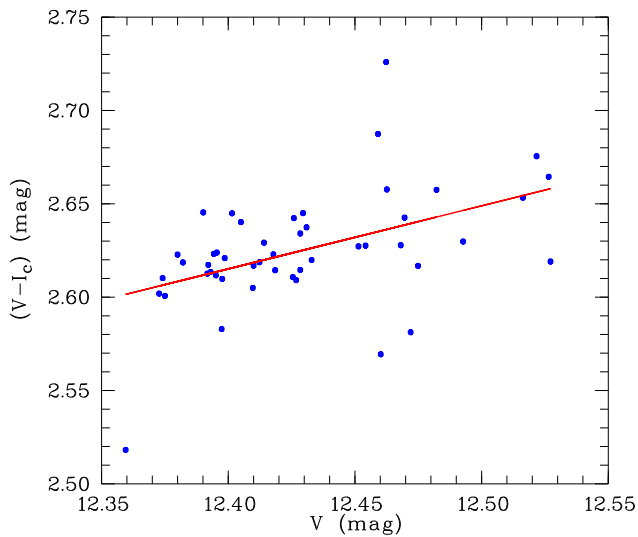


Figure 12. $V - I_c$ colour of Wray 15-906 as a function of the V magnitude. The solid (red) line is the least squares linear fit.

2016 to examine whether Wray 15-906 has experienced LBV excursions in the Hertzsprung-Russell diagram during this time period, in which case the star is expected to become bluer (hotter) with the brightness decrease and redder (cooler) when its brightness increases (e.g. van Genderen 1982; see also figs 5 and 6 in Kniazev et al. 2016). Fig. 12 plots the $V - I_c$ colour of Wray 15-906 as function of the V magnitude. What we see is that the star becomes redder with the brightness decrease, which is opposite to what one expects for the LBV excursions. This effect is also evident in

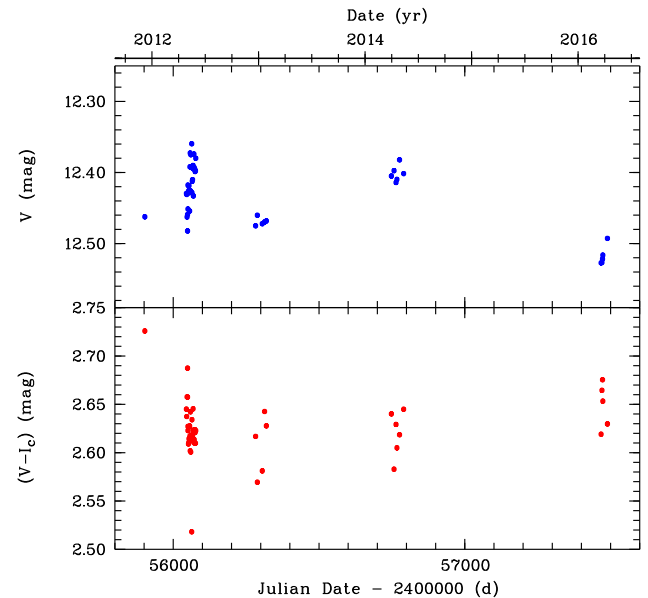


Figure 13. Upper panel: Light curve of Wray 15-906 in the V band in 2012–2016. Bottom panel: Evolution of the $V - I_c$ colour of Wray 15-906 with time.

Fig. 13 showing changes in the V magnitude and the $V - I_c$ colour with time. Since we did not detect noticeable changes in the spectral appearance of the star (meaning that T_{eff} was almost constant during our observations), we attribute the changes in the colour to variability of circumstellar extinction, probably caused by variability of the mass-loss rate.

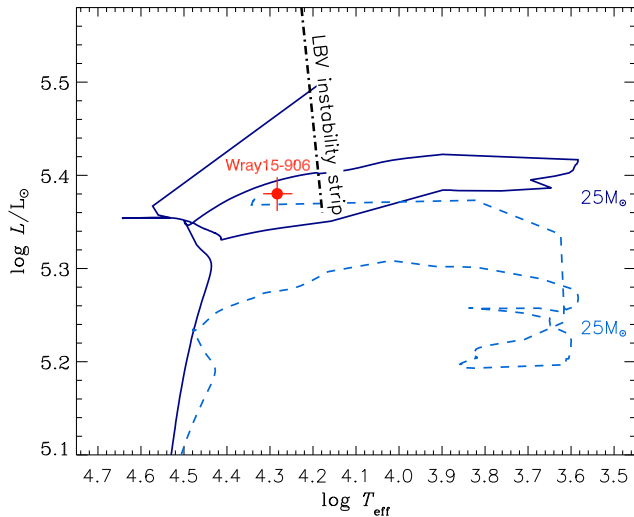


Figure 14. Position of Wray 15-906 in the Hertzsprung-Russell diagram (red dot with error bars). The dashed and solid lines show the Geneva evolutionary tracks of a $25 M_{\odot}$ single, solar-metallicity star with initial rotational velocities of 0 and 40 per cent of breakup, respectively (Ekström et al. 2012). The dot-dashed line marks the location of the LBV instability strip as defined in Groh et al. (2009a).

6 DISCUSSION

6.1 Evolutionary status and possible fate of Wray 15-906

Fig. 14 shows the position of Wray 15-906 in the Hertzsprung-Russell diagram for the adopted distance of 3.53 kpc along with the Geneva evolutionary tracks of single, solar-metallicity non-rotating and rotating (at 40 per cent of breakup) stars with initial mass of $M_{\text{init}} = 25 M_{\odot}$ (Ekström et al. 2012). If Wray 15-906 was born single, then its initial mass could be estimated to be $25 M_{\odot}$, which is close to the minimum mass for single (non-rotating) stars to become a Wolf-Rayet star (e.g. Georgy et al. 2012). According to the Geneva models, a star of this M_{init} loses about 70 per cent of its mass during the red supergiant phase and then evolves blueward in the Hertzsprung-Russell diagram to become a Wolf-Rayet star.

The surface He abundance (65 per cent by mass) derived for Wray 15-906 is typical of LBVs (e.g. Crowther 1997) and is intermediate between that of O and Wolf-Rayet stars. This suggests that Wray 15-906 has already gone through the red supergiant phase and currently is near the end of the He-burning stage, and implies the evolutionary age of this star of $\approx 7 - 8$ Myr. As a blue supergiant evolving from the red supergiant stage, Wray 15-906 should be subject to radial pulsations (e.g. Saio, Georgy & Meynet 2013; Jeffery & Saio 2016), which could be responsible for the heliocentric radial velocity variability in this star (see Table 4) and for its brightness variations on time-scales of the order of 100 d.

If Wray 15-906 was born with a low rotational velocity then it would need only several 1000 yr to finish its life with a supernova explosion (Georgy et al. 2012). The possibility that Wray 15-906 may soon explode is indirectly supported by the curious finding by Groh, Meynet & Ekström (2013a) and Groh et al. (2013b) that single stars with

Table 5. Comparison of Wray 15-906 with non-rotating (‘nr’) and rotating (‘r’) $25 M_{\odot}$ model stars at the pre-supernova stage from Ekström et al. (2012) and Groh et al. (2013b).

	Wray 15-906	nr	r
$\log(L_*/L_{\odot})$	5.36–5.40	5.38	5.50
T_* (kK)	23–27	27.1	24.6
T_{eff} (kK)	17.7–20.7	26.3	20.9
He (mass fraction)	0.63–0.67	0.83	0.93
C (mass fraction) (10^{-5})	≤ 6	6.8	16
N (mass fraction) (10^{-3})	2.7–3.5	8.2	16
O (mass fraction) (10^{-4})	0.8–1.6	1.1	6.5

$M_{\text{init}} = 20 - 25 M_{\odot}$ have LBV-like spectra before exploding as a supernova. Although unexpected, this finding conforms with previous claims (e.g. Kotak & Vink 2006) that LBVs could be the immediate precursors of supernovae.

Groh et al. (2013a,b) used the stellar evolution models by Ekström et al. (2012) as input in CMFGEN stellar atmosphere models to compute synthetic optical spectra and photometry (absolute magnitudes, colours and bolometric corrections) in different filters at the pre-supernova stage for stars with $M_{\text{init}} = 9 - 120 M_{\odot}$. They found that pre-supernova spectra of rotating models with $M_{\text{init}} = 20 - 25 M_{\odot}$ are very similar to those of bona-fide LBVs, such as P Cygni and AG Car. They also found that their non-rotating model with $M_{\text{init}} = 25 M_{\odot}$ appears at death as a WN11h star, such as Wray 15-682 or AG Car at its visual minimum. In this connection, we recall (see Section 4.1 and Fig. 4) that the spectrum of Wray 15-906 bears a strong resemblance with that of Wray 15-682, which given the blueward evolution of Wray 15-906 suggests that this star may end its life as a WN11h star.

In Table 5, we compare some parameters of Wray 15-906 with corresponding parameters of non-rotating and rotating (at 40 per cent of breakup) $25 M_{\odot}$ models at the pre-supernova stage compiled from Ekström et al. (2012) and Groh et al. (2013b)⁷. One can see that most parameters of Wray 15-906 agree fairly well with parameters of the non-rotating model with the main difference being that the model star appears hotter and its He abundance is much higher, which is however expectable because after the post-He-burning stage the temperature and the mass fraction of He at the surface of non-rotating stars increase to their pre-supernova values on a time scale of ~ 1000 yr. Table 5 also shows that the N abundance derived for Wray 15-906 is about a factor of two lower than what follows from the non-rotating model. Although this discrepancy, at least in part, may be due to a flaw in our spectral modelling, it should be noted that abundances predicted by stellar evolution models are very sensitive to the adopted prescriptions for convection, rotational mixing and mass-loss rates, which are still not well known and understood. We therefore speculate that Wray 15-906 may soon turn into a WN11h star before core collapse. If our speculation is correct, then one can expect that Wray 15-906 will explode as a supernova before its cir-

⁷ Note a misprint in table 3 of this paper, where the N abundance in the rotating $25 M_{\odot}$ model should have a tenfold higher value.

cumstellar shell dissipates into the interstellar medium. In this case, after ~ 100 yr the supernova blast wave will catch up and interact with the shell to produce a pc-scale supernova remnant.

It should be noted, however, that recent studies of red supergiants in star clusters (Beasor et al. 2020 and references therein) suggest that their mass-loss rates are more than an order of magnitude lower than those adopted in Ekström et al. (2012) and Groh et al. (2013a,b). If correct, this result would imply that during the red supergiant phase single stars did not lose enough mass to evolve blueward. However, it did not exclude the possibility that these stars can experience episodes of extreme mass-loss at the end of the red supergiant phase (e.g. Yoon & Cantiello 2010) or during the subsequent yellow hypergiant phase in the course of excursions on the cool side of the yellow void (de Jager & Nieuwenhuijzen 1997). Moreover, the mass loss required for the blueward evolution could also be driven by a companion star (e.g. through common-envelope ejection), which is quite possible given the high proportion of binaries among massive stars (Sana et al. 2012). The presence of the circumstellar shell around Wray 15-906 indicates that this star may have suffered mass loss at high rate in the recent past. To prove this, let us estimate the mass of this shell.

6.2 Mass of the circumstellar shell

To estimate the mass of the shell, we measured its flux densities at 22 and 70 μm using an 135 arcsec aperture centred on Wray 15-906. After subtraction contributions from the star and background emission, we found $F_\nu = 0.80 \pm 0.01$ Jy at 22 μm and $F_\nu = 9.04 \pm 0.94$ Jy at 70 μm . With these fluxes in hands, one can estimate the mass, M_d , and temperature, T_d , of the dust in the shell using the following relationship (Hildebrand 1983):

$$M_d = \frac{F_\nu d^2}{B(\nu, T_d) \kappa_\nu}, \quad (1)$$

where $B(\nu, T_d)$ is the Planck function and κ_ν is the mass absorption coefficient at frequency ν , which for $\lambda > 10 \mu\text{m}$ is given by (Laor & Draine 1993; Meikle et al. 2007):

$$\kappa_\nu \approx 1000 \left(\frac{\lambda}{20 \mu\text{m}} \right)^{-2} \text{ cm}^2 \text{ g}^{-1}. \quad (2)$$

Using equations (1) and (2) for the wavelengths 22 and 70 micron, one finds $T_d \approx 55 \pm 1$ K, while adopting $d \approx 3.53$ kpc results in $M_d \approx (1.45 \pm 0.25) \times 10^{-2} M_\odot$. The later estimate translates into the mass of the shell of $M_{\text{sh}} \approx 2.9 \pm 0.5 M_\odot$ if one assumes the gas-to-dust mass ratio of 200 (typical of Galactic red supergiants; Maun & Josselin 2011). Interestingly, the mass and radius (≈ 1 pc) of the shell around Wray 15-906 are similar to those of the shell around Wray 15-682 of, respectively, $2 \pm 1 M_\odot$ and ≈ 1 pc (Smith et al. 1994). This further strengthens the similarity between the two stars and makes it reasonable to assume that the kinematic ages of both shells are similar as well ($\sim 10,000$ yr; Smith et al. 1994).

6.3 Wray 15-906 as a runaway

Like the majority of (c)LBVs, Wray 15-906 is located outside of known star clusters and therefore is likely a runaway star (Gvaramadze et al. 2012b). Since *Gaia* DR2 provides accurate proper motion measurements for Wray 15-906 (see Table 1), it is tempting to calculate its past trajectory and to search for its possible parent star cluster. For this we used the solar peculiar motion of $(U_\odot, V_\odot, W_\odot) = (11.1, 12.2, 7.3) \text{ km s}^{-1}$ (Schönrich, Binney & Dehnen 2010) and the solar Galactocentric distance of $R_0 = 8.0$ kpc and the circular Galactic rotation velocity of $\Theta_0 = 240 \text{ km s}^{-1}$ (Reid et al. 2009). Table 6 gives the peculiar velocity components along the Galactic longitude (v_l) and latitude (v_b), and the peculiar transverse velocity of Wray 15-906 of $v_{\text{tr}} = (v_l^2 + v_b^2)^{1/2}$ for three values of the distance. To this table we also added the peculiar radial velocity (v_r) of Wray 15-906, derived under the assumption that the heliocentric radial velocity of this star is equal to zero (see Section 4.2), and the total space velocity (v_*) of the star. For the error calculation, only uncertainties in the proper motion measurements were taken into account. Note that the total space velocity of Wray 15-906 only weakly depends on the distance. One can show that for d ranging from, say, 2 to 6 kpc, v_* ranges from ≈ 20 to 30 km s^{-1} .

Table 6 shows that Wray 15-906 is moving almost parallel to the Galactic plane with a velocity of $\approx 20 - 25 \text{ km s}^{-1}$. The total space velocity of Wray 15-906 of $\approx 30 \text{ km s}^{-1}$ is typical of classical runaway stars (Blaauw 1961). In Fig. 15, we plot the past trajectory of Wray 15-906 over a time period of 7 Myr. Inspection of the WEBDA⁸ data base (Mermilliod 1995) showed that there are two young star clusters, [KPR2004b] 294⁹ and C 1128-631, whose approximate boundaries (shown by dashed blue circles of radius of $0^\circ 25'$; Piskunov et al. 2007) are crossed by the trajectory of Wray 15-906. According to WEBDA, [KPR2004b] 294 and C 1128-631 are located at the distances of 2.74 and 3.40 kpc, and their ages are ≈ 4.4 and 15 Myr, respectively. Although, due to the zero-point problem in the *Gaia* DR2 parallaxes (e.g. Lindegren et al. 2018), one cannot rule out the possibility that Wray 15-906 is located at the same distance as [KPR2004b] 294, the much younger age of the latter makes the physical relationship between the two objects unlikely. Moreover, at the shorter distance the evolutionary age of Wray 15-906 (implied by the He abundance on the surface of this star) would be higher, which makes the age discrepancy even more worse.

The distance to C 1128-631 is in a good agreement with that to Wray 15-906, but the cluster is a factor of about two older than the star. This implies that either the two objects are not related to each other or that Wray 15-906 is a rejuvenated product of binary evolution, i.e. a blue straggler (e.g. Vanbeveren et al. 2013; Langer & Kudritzki 2014; Podsiadlowski & Vink 2014). In this case, the star most likely will not evolve through the red supergiant phase and will remain in the blue part of the Hertzsprung-Russell diagram. Also, one cannot exclude the possibilities that the parent cluster of Wray 15-906 has already dissolved or that this star has

⁸ <http://webda.physics.muni.cz/>

⁹ It is believed (Schilbach & Röser 2008) that [KPR2004b] 294 is the birth cluster of the O6.5 III(f) runaway star HD 96946.

Table 6. Kinematic data on Wray 15-906 (see text for details).

d (kpc)	v_l (km s^{-1})	v_b (km s^{-1})	v_r (km s^{-1})	v_{tr} (km s^{-1})	v_* (km s^{-1})
3.00	19.0 ± 1.3	5.5 ± 1.0	18.5	19.8 ± 1.3	27.1
3.53	21.8 ± 1.5	5.2 ± 1.2	19.3	24.4 ± 1.4	31.1
4.27	25.7 ± 1.8	4.6 ± 1.5	18.2	26.1 ± 1.8	31.8

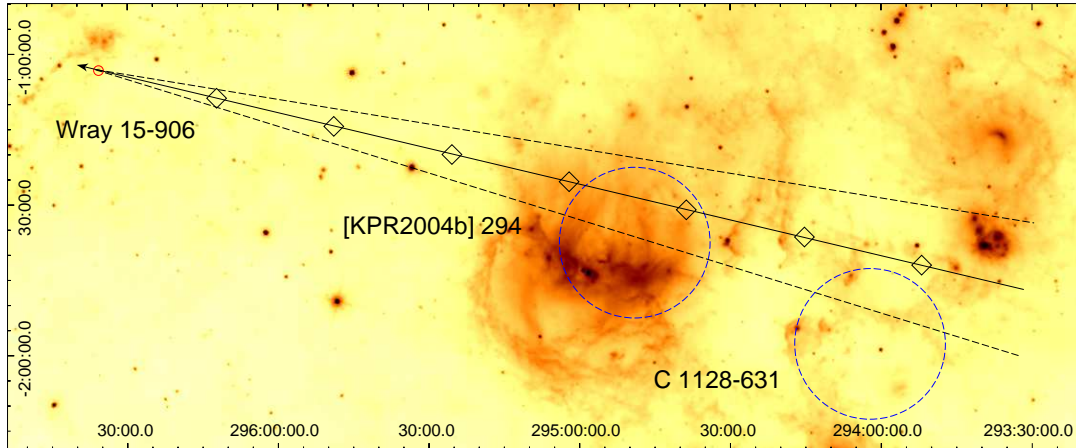


Figure 15. *WISE* 22 μm image of the field containing Wray 15-906 (marked by a red circle) and two open star clusters [KPR2004b] 294 and C 1128-631 (indicated by dashed blue circles). The arrow shows the direction of motion of Wray 15-906 for $d = 3.53$ kpc. A solid line shows the trajectory of Wray 15-906 with 1σ uncertainties shown by dashed lines. Diamonds mark the positions of Wray 15-906 over a time period of 7 Myr with a time step of 1 Myr. The image is oriented with Galactic longitude (in units of degrees) increasing to the left and Galactic latitude increasing upwards. At the distance of 3.53 kpc, 1° corresponds to ≈ 60.7 pc.

found itself in the field because of the two-step-ejection process, i.e. due to the dissolution of a runaway massive binary (Pflamm-Altenburg & Kroupa 2010). In the latter case, the parent cluster cannot be determined at all.

Finally, we note that the central location of Wray 15-906 within the almost perfectly circular shell implies that the shell does not feel the ram pressure of the interstellar medium caused by the motion of the star. This could be understood if the nebula was ejected (almost) instantly (e.g. due to some catastrophic event in the underlying star or due to a brief episode of high mass loss), in which case the ejecta should be massive enough not to feel the ambient medium. This implies that the mass of the shell should be much larger than the mass of the interstellar medium displaced by the shell. Adopting $M_{sh} = 2.9 M_\odot$, one finds that the number density of the interstellar medium should be $\ll 20 \text{ cm}^{-3}$. Alternatively, the shell around Wray 15-906 could be the result of interaction between the current stellar wind and a co-moving dense material lost by the star during the preceding red supergiant phase. In this case, the wind-wind interaction region (shell) could be shielded from the ram pressure of the interstellar medium by the external material of the red supergiant wind (cf. Gvaramadze et al. 2019a).

7 SUMMARY

We have presented the results of study of the new Galactic cLBV Wray 15-906 discovered via the detection of its circular circumstellar shell with *WISE* and *Herschel*, and follow-up spectroscopy with SALT. Our long-slit and échelle spectroscopic monitoring of Wray 15-906 lasting 8 years (from 2012 February to 2020 February) did not reveal significant changes in the spectrum of this star, but resulted in detection of moderate variability in the intensities and P Cygni absorption profiles of some lines, which is typical of hot stars with extended atmospheres. Also, we did not find significant changes in the brightness of Wray 15-906 over the time period from 2001 to 2019. The *V*-band light curve constructed using archival and our own photometric observations revealed quasi-periodic variability with a period of ≈ 1700 d and an amplitude of ≈ 0.1 mag. We analysed one of the échelle spectra of Wray 15-906 with the stellar atmosphere code CMFGEN, obtaining a stellar temperature of 25 kK. Wray 15-906 is highly reddened, $E(B - V) \approx 2$ mag. Using the *Gaia* DR2 distance to Wray 15-906 of 3.53 kpc, we derived the stellar luminosity of $\log(L/L_\odot) \approx 5.4$ and the mass-loss rate of $\approx 3 \times 10^{-5} M_\odot \text{ yr}^{-1}$. The stellar wind composition is dominated by helium (≈ 65 per cent by mass), implying that Wray 15-906 is a blueward evolving post-red supergiant star. If Wray 15-906 was born single, then its initial mass was $25 M_\odot$, which is close to the minimum mass for single (non-rotating) stars to become a Wolf-Rayet star. We have speculated that Wray 15-906 may soon transform into

a WN11h star to explode as a supernova after ~ 1000 yr. We estimated the dust temperature and mass in the circumstellar shell to be ≈ 55 K and $0.015 M_{\odot}$, respectively, implying the mass of the shell of about $3 M_{\odot}$ for the gas-to-dust mass ratio of 200. The presence of the shell of this mass indicates that Wray 15-906 has experienced a substantial mass loss in the recent past, which allowed this star to evolve blueward in the Hertzsprung-Russell diagram. We have calculated the peculiar transverse velocity of Wray 15-906 to be $\approx 25 \text{ km s}^{-1}$ using *Gaia* DR2 proper motion measurements and searched for the possible parent star cluster for this star within the error cone of its past trajectory. We found that about 7 Myr ago, the trajectory of Wray 15-906 passed through the open star cluster C1128-631, whose age is about twice the age of the star, meaning that the two objects could be associated with each other if Wray 15-906 is a rejuvenated product of binary evolution (a blue straggler).

8 ACKNOWLEDGEMENTS

This work is based on observations obtained with the Southern African Large Telescope (SALT), programmes 2013-1-RSA_OTH-014, 2013-2-RSA_OTH-003, 2015-1-SCI-017, 2016-1-SCI-012, 2017-1-SCI-006 and 2018-1-MLT-008, and supported by the Russian Foundation for Basic Research grant 19-02-00779. O.M. acknowledges support from the Czech Science Foundation GA18-05665S. A.Y.K. acknowledges support from the National Research Foundation (NRF) of South Africa. We are grateful to F. Najarro for useful discussion and for providing us with a CMFGEN model of P Cygni. This research has made use of the NASA/IPAC Infrared Science Archive, which is operated by the Jet Propulsion Laboratory, California Institute of Technology, under contract with the National Aeronautics and Space Administration, the SIMBAD data base and the VizieR catalogue access tool, both operated at CDS, Strasbourg, France, the WEBDA data base, operated at the Department of Theoretical Physics and Astrophysics of the Masaryk University, and data from the European Space Agency (ESA) mission *Gaia* (<https://www.cosmos.esa.int/gaia>), processed by the *Gaia* Data Processing and Analysis Consortium (DPAC, <https://www.cosmos.esa.int/web/gaia/dpac/consortium>). Funding for the DPAC has been provided by national institutions, in particular the institutions participating in the *Gaia* Multilateral Agreement.

9 DATA AVAILABILITY

The data underlying this article will be shared on reasonable request to the corresponding authors.

REFERENCES

- Alfonso-Garzón J., Domingo A., Mas-Hesse J. M., Giménez A., 2012, *A&A*, 548, A79
- Barnes S. I. et al., 2008, in McLean I. S., Casali M. M., eds, Proc. SPIE Conf. Ser. Vol. 7014, Ground-based and Airborne Instrumentation for Astronomy II. SPIE, Bellingham, p. 70140K
- Beasar E. R., Davies B., Smith N., van Loon J. T., Gehr R. D., Figer D. F., 2020, *MNRAS*, 492, 5994
- Benjamin R. A. et al., 2003, *PASP*, 115, 953
- Berdnikov L. et al., 2012, *Astronomy Reports*, 56, 290
- Blaauw A., 1961, *Bull. Astron. Inst. Netherlands*, 15, 265
- Boffin H. M. J. et al., 2016, *A&A*, 593, A90
- Bohannan B., 1997, in Nota A., Lamers H. J. G. L. M., eds, ASP Conf. Ser. Vol. 120, Luminous Blue Variables: Massive Stars in Transition. Astron. Soc. Pac., San Francisco, p. 120
- Bramall D. G. et al., 2010, in McLean I. S., Ramsay S. K., Takami H., eds, Proc. SPIE Conf. Ser. Vol. 7735, Ground-based and Airborne Instrumentation for Astronomy III. SPIE, Bellingham, p. 77354F
- Bramall D. G. et al., 2012, in McLean I. S., Ramsay S. K., Takami H., eds, Proc. SPIE Conf. Ser. Vol. 8446, Ground-based and Airborne Instrumentation for Astronomy IV. SPIE, Bellingham, p. 84460A
- Buckley D. A. H., Swart G. P., Meiring J. G., 2006, *Proc. SPIE*, 6267, 32
- Burgh E. B., Nordsieck K. H., Kobulnicky H. A., Williams T. B., O'Donoghue D., Smith M. P., Percival J. W., 2003, *Proc. SPIE*, 4841, 1463
- Burgemeister S., Gvaramadze V., Stringfellow G. S., Kniazev A. Y., Todt H., Hamann W.-R., 2013, *MNRAS*, 429, 3305
- Chentsov E. L., Maryeva O. V., 2016, *Astrophysical Bulletin*, 71, 279
- Clark J. S., Larionov V. M., Arkharov A., 2005, *A&A*, 435, 239
- Cochetti Y. R., Kraus M., Arias M. L., Cidale L. S., Eemäe T., Liimets T., Torres A. F., Djupvik A. A., 2020, *AJ*, in press (arXiv:2008.11017)
- Conti P. S., 1984, in Maeder A., Renzini A., eds, *Observational Tests of the Stellar Evolution Theory*. Reidel, Dordrecht, p. 233
- Cox A. N., 2000, *Allen's Astrophysical Quantities*. Am. Inst. Phys., New York
- Cox N. L. G. et al., 2012, *A&A*, 537, A35
- Crause L. A. et al., 2014, in Ramsay S. K., McLean I. S., Takami H., eds, Proc. SPIE Conf. Ser. Vol. 9147, Ground-based and Airborne Instrumentation for Astronomy V. SPIE, Bellingham, p. 91476T
- Crawford S. M. et al., 2010, in Silva D. R., Peck A. B., Soifer B. T., eds, Proc. SPIE Conf. Ser. Vol. 7737, Observatory Operations: Strategies, Processes, and Systems III. SPIE, Bellingham, p. 773725
- Crowther P. A., 1997, in Nota A., Lamers H. J. G. L. M., eds, ASP Conf. Ser. Vol. 120, Luminous Blue Variables: Massive Stars in Transition. Astron. Soc. Pac., San Francisco, p. 51
- Cutri R. M. et al., 2003, *VizieR Online Data Catalog*, 2246, 0
- Cutri R. M. et al., 2014, *VizieR Online Data Catalog: II/328*, 2328, 0
- Davidson K., 2020, *Galaxies*, 8, 10
- de Jager C., Nieuwenhuijzen H., 1997, *MNRAS*, 290, 50
- Ekström S. et al., 2012, *A&A*, 537, A146
- Fazio G. G. et al., 2004, *ApJS*, 154, 10
- Fitzpatrick E. L., 1999, *PASP*, 111, 63
- Flagey N., Noriega-Crespo A., Petric A. O., Geballe T. R., 2014, *AJ*, 148, 34
- Fullerton A. W., Massa D. L., Prinja R. K., Owocki S. P., Cranmer S. R., 1997, *A&A*, 327, 699
- Gaia* Collaboration, Brown A. G. A., Vallenari A., Prusti T., de Bruijne J. H. J., Babusiaux C., Bailer-Jones C. A. L., 2018, *A&A*, 616, A1
- Georgy C., Ekström S., Meynet G., Massey P., Levesque E. M., Hirschi R., Eggenberger P., Maeder A., 2012, *A&A*, 542, A29
- Groh J. H. et al., 2009a, *ApJ*, 705, L25
- Groh J. H., Hillier D. J., Daminieli A., Whitelock P. A., Marang F., Rossi C., 2009b, *ApJ*, 698, 1698
- Groh J. H., Vink J. S., 2011, *A&A* 531, L10

- Groh J. H., Meynet G., Ekström S., 2013a, *A&A*, 550, L7
- Groh J. H., Meynet G., Georgy C., Ekström S., 2013b, *A&A*, 558, A131
- Groh J., Meynet G., Ekström S., Georgy C., 2014, *A&A*, 564, A30
- Gvaramadze V. V., Kniazev A. Y., 2017, in Miroshnichenko A.S., Zharikov S.V., Korcakova D., Wolf M., eds, ASP Conf. Ser. Vol. 508, The B[e] Phenomenon. Forty Years of Studies. Astron. Soc. Pac., San Francisco, p. 207
- Gvaramadze V. V. et al., 2009, *MNRAS*, 400, 524
- Gvaramadze V. V., Kniazev A. Y., Fabrika S., Sholukhova O., Berdnikov L. N., Cherepashchuk A. M., Zharova A. V., 2010a, *MNRAS*, 405, 520
- Gvaramadze V. V., Kniazev A. Y., Fabrika S., 2010b, *MNRAS*, 405, 1047
- Gvaramadze V. V., Kniazev A. Y., Kroupa P., Oh S., 2011, *A&A*, 535, A29
- Gvaramadze V. V. et al., 2012a, *MNRAS*, 421, 3325
- Gvaramadze V. V., Weidner C., Kroupa P., Pflamm-Altenburg J., 2012b, *MNRAS*, 424, 3037
- Gvaramadze V. V., Kniazev A. Y., Maryeva O. V., Berdnikov L. N., 2018, *MNRAS*, 474, 1412
- Gvaramadze V. V., Maryeva O. V., Kniazev A. Y., Alexashov D. B., Castro N., Langer N., Katkov I. Y., 2019a, *MNRAS*, 482, 4408
- Gvaramadze V. V., Gräfener G., Langer N., Maryeva O. V., Kniazev A. Y., Moskvitin A. S., Spiridonova O. I., 2019b, *Nature*, 569, 684
- Gvaramadze V. V., Pakhomov Yu. V., Kniazev A. Y., Ryabchikova T. A., Langer N., Fossati L., Grebel E. K., 2019c, *MNRAS*, 489, 5136
- Henize K. G., 1976, *ApJS*, 30, 491
- Hildebrand R. H., 1983, *QJRAS*, 24, 267
- Hillier D. J., 1991, *A&A*, 247, 455
- Hillier D. J., Miller D. L., 1998, *ApJ*, 496, 407
- Hillier D. J., Miller D. L., 1999, *ApJ*, 519, 354
- Hillier D. J., Davidson K., Ishibashi K., Gull T., 2001, *ApJ*, 553, 837
- Humphreys R. M., Davidson K., 1994, *PASP*, 106, 1025
- Hutsemékers D., Cox N. L. J., Vamvatira-Nakou C., 2013, *A&A*, 552, L6
- Jeffery C. S., Saio H., 2016, *MNRAS*, 458, 1352
- Justham S., Podsiadlowski P., Vink J. S., 2014, *ApJ*, 796, 121
- Kaper L., Henriks H. F., Nichols J. S., Snoek L. C., Volten H., Zwarthoed G. A. A., 1996, *A&AS*, 116, 257
- Kaufer A., Stahl O., Wolf B., Gaeng T., Gummertsbach C. A., Kovacs J., Mandel H., Szeifert T., 1996, *A&A*, 305, 887
- Kniazev A. Y., Gvaramadze V. V., 2015, Proceedings of the SALT Science Conference 2015 (SSC2015). Stellenbosch Institute of Advanced Study, South Africa, p. 49
- Kniazev A. Y., Pustilnik S. A., Grebel E. K., Lee H., Pramskij A. G., 2004, *ApJS*, 153, 429
- Kniazev A. Y., Gvaramadze V. V., Berdnikov L. N., 2015, *MNRAS*, 449, L60
- Kniazev A. Y., Gvaramadze V. V., Berdnikov L. N., 2016, *MNRAS*, 459, 3068
- Kniazev A. Y. et al., 2008, *MNRAS*, 388, 1667
- Kniazev A. Y., Usenko I. A., Kovtyukh V. V., Berdnikov L. N., 2019, *Astrophys. Bull.*, 74, 208
- Kniazev A. Y., Gvaramadze V. V., Berdnikov L. N., 2017, in Balega Y. Y., Kudryavtsev D. O., Romanyuk I. I., Yakunin I. A., eds, ASP Conf. Ser. Vol. 510, Stars: From Collapse to Collapse. Astron. Soc. Pac., San Francisco, p. 480
- Kobulnicky H. A., Nordsieck K. H., Burgh E. B., Smith M. P., Percival J. W., Williams T. B., ODonoghue D., 2003, *Proc. SPIE*, 4841, 1634
- Kobulnicky H. A. et al., 2016, *ApJS*, 227, 18
- Kochanek C. S. et al., 2017, *PASP*, 129, 104502
- Kotak R., Vink, J. S., 2006, *A&A*, 460, L5
- Kronberger M. et al., 2016, *JPhCS*, 728, 072012
- Lamers H. J. G. L. M., Korevaar P., Cassatella A., 1985, *A&A*, 149, 29
- Langer N., Kudritzki R. P., 2014, *A&A*, 564, A52
- Langer N., Hamann W.-R., Lennon M., Najarro F., Pauldrach A. W. A., Puls J., 1994, *A&A*, 290, 819
- Laor A., Draine B. T., 1993, *ApJ*, 402, 441
- Lindegren L. et al., 2018, *A&A*, 616, A2
- Lobel A., Martayan C., Corcoran M., Groh J. H., Frémat Y., 2015, in Meynet G., Georgy C., Groh J., Stee P., eds, Proc. IAU Symp. 307, New Windows on Massive Stars: Asteroseismology, Interferometry, and Spectropolarimetry. Cambridge Univ. Press, Cambridge, p. 115
- Lomb N. R., 1976, *Ap&SS*, 39, 447
- Markova N., Valchev T., 2000, *A&A*, 363, 995
- Mauerhan J. C., Wachter S., Morris P. W., Van Dyk S. D., Hoard D. W., 2010, *ApJ*, 724, L78
- Mauron N., Josselin E., 2011, *A&A*, 526, A156
- Meikle W. P. S. et al., 2007, *ApJ*, 665, 608
- Mermilliod J. C., 1995, in Egret D., Albrecht M., eds, Information and Online Data in Astronomy. Kluwer, Dordrecht, p. 127
- Mizuno D. R. et al., 2010, *AJ*, 139, 1542
- Moultaka J., Ilovaisky S. A., Prugniel P., Soubiran C., 2004, *PASP*, 116, 693
- Najarro F., Figer D. F., Hillier D. J., Geballe T. R., Kudritzki R. P., 2009, *ApJ*, 691, 1816
- Najarro F., Hanson M. M., Puls J., 2011, *A&A*, 535, A32
- Nota A., Livio M., Clampin M., Schulte-Ladbeck R., 1995, *ApJ*, 448, 788
- O'Donoghue D. et al., 2006, *MNRAS*, 372, 151
- Ochsendorf B. B., Cox N. L. J., Krijt S., Salgado F., Berné O., Bernard J. P., Kaper L., Tielens A. G. G. M., 2014, *A&A*, 563, A65
- Parker Q. A. et al., 2005, *MNRAS*, 362, 689
- Peri C. S., Benaglia P., Brookes D. P., Stevens I. R., Isequilla N. L., 2012, *A&A*, 538, 108
- Pflamm-Altenburg J., Kroupa P., 2010, *MNRAS*, 404, 1564
- Pilbratt G. L. et al., 2010, *A&A*, 518, L1
- Piskunov A. E., Schilbach E., Kharchenko N. V., Röser S., Scholz R.-D., 2007, *A&A*, 468, 151
- Pojmanski G., 1997, *Acta Astronomica*, 47, 467
- Puls J., Markova N., Scuderi S., Stanghellini C., Taranova O. G., Burnley A. W., Howarth I. D., 2006, *A&A*, 454, 625
- Richardson N. D., Mehner A., 2018, *Res. Notes Am. Astron. Soc.*, 2, 121
- Richardson N. D., Gies D. R., Williams S. J., 2011, *AJ*, 142, 201
- Saio H., Georgy C., Meynet G., 2013, *MNRAS*, 433, 1246
- Sana H. et al., 2012, *Science*, 337, 444
- Scargle J. D., 1982, *ApJ*, 263, 835
- Schilbach E., Röser S., 2008, *A&A*, 489, 105
- Shappee B. J. et al., 2014, *ApJ*, 788, 48
- Silva K. M., Flagey N., Noriega-Crespo A., Carey S., Ingallinera A., 2017, *AJ*, 153, 115
- Skrutskie M. F. et al., 2006, *AJ*, 131, 1163
- Smith L. J., Crowther P. A., Prinja R. K., 1994, *A&A*, 281, 833
- Smith N., 2014, *ARA&A*, 52, 487
- Smith N., Vink J. S., de Koter A., 2004, *ApJ*, 615, 475
- Smith N., Aghakhanloo M., Murphy J. W., Drout M. R., Stassun K. G., Groh J. H., 2019, *MNRAS*, 488, 17
- Spitzer Science Center, 2009, *VizieR Online Data Catalog*, 2293, 0
- Stahl O., Mandel H., Szeifert Th., Wolf B., Zhao F., 1991, *A&A*, 244, 467
- Stahl O., Mandel H., Wolf B., Gaeng Th., Kaufer A., Kneer R., Szeifert Th., Zhao F., 1993, *A&AS*, 99, 167
- Stahl O., Jankovics I., Kovacs J., Wolf B., Schmitz W., Kaufer A., Rivinius T., Szeifert T., 2001, *A&A*, 375, 54

- Stenholm B., 1975, *A&A*, 39, 307
- Stephenson C. B., Sanduleak N., 1971, *Pub. Warner Swasey Obs.*, 1, 1
- Stothers R. B., Chin C.-W., 1996, *ApJ*, 468, 842
- Stringfellow G. S., Gvaramadze V. V., Beletsky Y., Kniazev A. Y., 2012a, in Richards M. T., Hubeny I., eds, *Proc. IAU Symp.* 282, *From Interacting Binaries to Exoplanets: Essential Modelling Tools*. Cambridge Univ. Press, Cambridge, p. 267
- Stringfellow G. S., Gvaramadze V. V., Beletsky Y., Kniazev A. Y., 2012b, in Drissen L., St-Louis N., Robert C., Moffat A. F. J., eds, *ASP Conf. Ser. Vol. 465, Four Decades of Massive Star Research A Scientific Meeting in Honor of Anthony J. Moffat*. Astron. Soc. Pac., San Francisco, p. 514
- van Genderen A. M., 2001, *A&A*, 366, 508
- Vanbeveren C., Mennekens N., Van Rensbergen W., De Loore C., 2013, *A&A*, 552, A105
- Vink J. S., 2012, in Davidson K., Humphreys R. M., eds, *Astrophysics and Space Science Library, Vol. 384, Eta Carinae and the Supernova Impostors*. Springer, New York, p. 221
- Wachter S., Mauerhan J. C., van Dyk S. D., Hoard D. W., Kafka S., Morris P. W., 2010, *AJ*, 139, 2330
- Wachter S., Mauerhan J., van Dyk S., Hoard D. W., Morris P., 2011, *Bull. Soc. R. Sci. Liège*, 80, 291
- Weis K., 2001, *Rev. Mod. Astron.*, 14, 261
- Weis K., Bomans D. J., 2020, *Galaxies*, 8, 20
- Werner M. W. et al., 2004, *ApJS*, 154, 1
- Wray J. D., 1966, PhD thesis, Northwestern Univ.
- Wright E. L. et al., 2010, *AJ*, 140, 1868
- Yoon S.-C., Cantiello M., 2010, *ApJ*, 717, L62